A Conduction-Cooled Superconducting Magnet System - Design, Fabrication and Thermal Tests

Xiaowei Song[1], Joachim Holbøll[1], Qiuliang Wang[2], Yingming Dai[2], Nenad Mijatovic[1] and Jiawei Wang[1]

1. Department of Electrical Engineering, Technical University of Denmark

2. Institute of Electrical Engineering, Chinese Academy of Sciences

Abstract

A conduction-cooled superconducting magnet system with an operating current of 105.5 A was designed, fabricated and tested for material processing applications. The magnet consists of two coaxial NbTi solenoid coils with an identical vertical height of 300 mm and is installed in a high-vacuumed cryostat. A two-stage GM cryocooler with a cooling power of 1.5 W at 4.2 K in the second stage is used to cool the system from room temperature to 4.2 K. In this paper, the detailed design, fabrication, thermal analysis and tests of the system are presented.

1. Introduction

Many research areas have benefited from the application of high field superconducting magnets. Particularly, magnetic field effects have recently been observed for material, chemical, and biological systems [1], [2]. A high field magnet system with a wide warm bore is convenient for researchers to carry out material processing experiments, because it provides enough space to install samples, as well as the cooling, heating and monitoring systems [3]. Conduction-cooled superconducting magnets have become increasingly popular in research and industry due to their ease and simplicity of operation as compared to traditional superconducting magnets immersed in liquid helium (LHe) [4], [5].

In 1983, Hoenig. M. first demonstrated a thermal design of the conduction-cooled superconducting magnet combined with GM cryocoolers [6]. However, due to the heat leakage through copper current leads, only Nb_3Sn superconductors could be used, and the magnet could only carry a current of 40 A. The development of high-temperature superconductors, along with the progress of cryocoolers, has enabled large-scale applications of conduction-cooled superconducting magnets [7]. It is expected that the conduction-cooled solution may replace the conventional solution utilizing liquid helium in the near future.

A conduction-cooled superconducting magnet system was designed, fabricated and tested for material processing applications in the Applied Superconductivity Laboratory, Institute of Electrical Engineering, Chinese Academy of Sciences (IEE, CAS). The magnet has a warm bore of Ø 250 mm and a maximum central field of 4.5 T. This paper presents the detailed design, fabrication, thermal analysis and tests. In addition, the AC losses generated during charging are estimated.

2. Design and Fabrication of the Superconducting Magnet System

2.1. Electromagnetic design

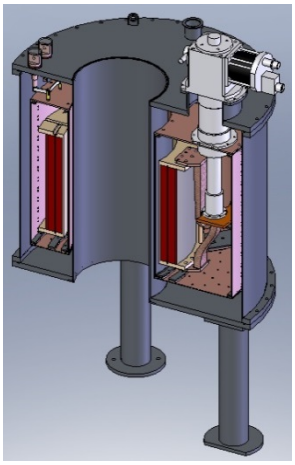

Fig. 1 – 3D cross-section of the superconducting magnet system

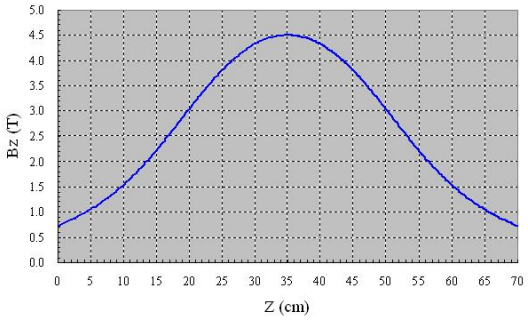

Fig. 2 – Flux density distribution along the central axis (Z=35 cm denotes the middle point of the magnet in the central axis)

The 3D cross-sectional view of the superconducting magnet system is illustrated in Fig. 1. Two NbTi solenoid coils are wound coaxially with an identical vertical height of 300 mm. The two coils are electrically connected in series, and a single power supply is used to provide the operating current of 105.5 A. Fig. 2 shows the flux density distribution along the central axis. The

maximum central field is 4.5 T, with 1.5 T contributed by the inner coil and 3 T by the outer coil. Detailed parameters are listed in Table 1.

Table 1 – Parameters of the superconducting magnet

	Magnet	Coils	
		Inner coil	Outer coil
Inner diameter (mm)	305	315	362
Outer diameter (mm)	450	352	409.5
Height (mm)	325	300	300
Number of turns	16128	5058	11070
Superconductors		NbTi/Cu	NbTi/Cu
Dimension of wires (mm)		Ø 1.05	Ø 0.80
Operating current (A)	105.5		
Maximum central field (T)	4.5	1.5	3
Inductance (H)	66.9		
Maximum field (T)	5.32	5.32	3.86

2.2. Fabrication and assembly

Wet-winding technology is adopted to fabricate the superconducting coils. The coils are wound onto a brass former, which not only has a robust mechanical strength but a relatively high thermal conductivity at 4.2 K [3]. The former has a 2 mm wide slot along the axial direction in order to reduce the eddy current loss during charging. A 1 mm thick polyimide insulation layer is coated on the outside surface of the brass former. The first layer of the inner coil is directly wound on the insulation layer but not bonded to it.

During the winding, the DW-3 epoxy resin is used to impregnate the coils and fill the space between superconducting wires. To improve the thermal conductivity, aluminium nitride (AlN) powder is added into the epoxy resin with a weight ratio of 1:2 [8]. 10 mm thick fiberglass saturated with epoxy resin is wound onto the outer surface of the inner coil, and the outer coil is then wound directly onto the fiberglass and bonded to it.

After the outer coil is finished, Ø 1 mm stainless steel wire is applied as an overbinding layer to support the electromagnetic force in the coils [4]. The coils are then moved to a furnace for curing. After 8 hours at 60℃, the epoxy is cured and the coils are ready to be assembled and installed in the cryostat.

The configuration of the system is schematically shown in Fig.3. The magnet is covered by a radiation shield and wrapped with multi-layer insulation (MLI) to minimize thermal radiation. An off-the-shelf two-stage GM cryocooler RDK-415D with 50 W at 50 K in the first stage and 1.5 W at 4.2 K in the second stage is used to cool the system. The first stage of the cold head is rigidly attached to the radiation shield, whereas the second stage is connected to the magnet through a flexible copper braid. This arrangement ensures the highest possible heat removal rate in the first stage where both temperatures and heat loads are greater, while still permitting different thermal contraction between components as the apparatus cools from room temperature [9]. During the assembly, 0.1 mm thick indium foils are placed between the contact surfaces to reduce the thermal contact resistance. The binary current lead, a combination of a copper conductor in the high-temperature section and an HTS conductor in the low-temperature section, is employed to reduce the heat load in the second stage [7]. The apparatus is installed in a vacuum vessel and suspended by G-10 supporting rods.

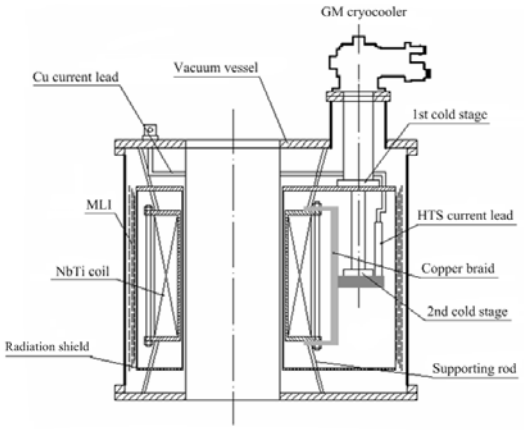

Fig. 3 – Configuration of the superconducting magnet system

3. Thermal analysis

To ensure the operating temperature, heat loads of the system must be limited. There are four different heat loads: thermal conduction through the supporting rods, thermal radiation, conduction heat leakage from residual gas, and heat transferred from current leads [10].

3.1. Heat loads calculation

Thermal conduction can be easily determined by Fourier's Law expressed below:

$$Q_c = \frac{A}{L}\int_{T_C}^{T_H} \lambda(T)dT \qquad (1)$$

where Q_c is the thermal conduction; T_H and T_C are the temperatures in the high and low-temperature terminal, respectively; A and L are the cross section area and the length of the component; $\lambda(T)$ is the temperature-dependent thermal conductivity. The thermal conductivity of different materials can be found in [11].

The radiation shield in the system operates at an intermediate temperature and 16 layers of MLI are wrapped around the shield. The radiation heat load can be calculated by:

$$Q_r = \frac{\varepsilon\sigma S}{(2-\varepsilon)(n+1)}(T_1^4 - T_2^4) \qquad (2)$$

where Q_r is the radiation heat load; ε is the emissivity of the material, the typical value of which is 0.05 [12]; σ is the Stefan-Boltzmann constant which equals 5.67

$\times 10^{-8}$ W· m^{-2}· K^{-4}; S denotes the area of the cold body and n is the number of layers of MLI; T_1 and T_2 represent the high and low temperatures, respectively. T_1 is 300 K and T_2 is around 50 K for calculating the heat load of the first stage, while T_1 is 50 K and T_2 is 4.2 K for calculating the heat load of the second stage.

The heat leakage of residual gas Q_g can be approximately given by:

$$Q_g = c_0 \alpha P \cdot S \cdot \Delta T \qquad (3)$$

where the constant c_0 is 1.2 for the air and the accommodation coefficient α is 0.5 [13]. P is pressure in the vacuum vessel, and $\Delta T = T_1 - T_2$ is the temperature difference.

The heat transferred from the copper current leads Q_{CL} is the sum of conduction heat and the Joule heat. It can be determined by:

$$Q_{CL} = I \cdot \sqrt{L_0 (T_H^2 - T_C^2)} \qquad (4)$$

where L_0 is Lorenz constant and it equals 2.445 × 10^{-8} W · Ω / K^2; I is the transporting current. T_H and T_C are 300 K and 50 K, respectively.

The HTS current leads are CSL12/80.3, supplied by CAN Superconductors, s.r.o. The heat leakage from 64 K to 4 K is 0.12 W per pair.

Through (1) to (4) and based on the specifications of the system, the heat loads of the first and second stages are determined to be 15.2 W and 0.3 W, respectively. The heat loads of each stage match the cooling capacity of the GM cryocooler with sufficient margin.

3.2. Thermal simulation

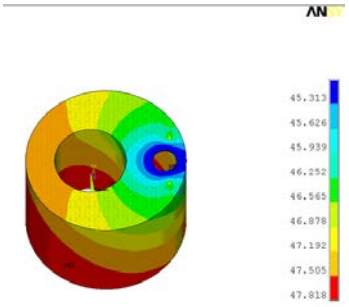

Fig. 4 – Temperature distribution in the shield. The left and right holes are the warm bore and the position of 1st stage of the cold head, respectively.

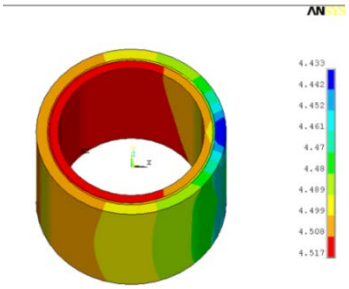

Fig. 5 – Temperature distribution in the superconducting coils

A finite element (FE) thermal model is built based on ANSYS software. SOLID90, a 3-D, 2nd-order, 20-node element is employed in the model [14]. Fig. 4 and Fig. 5 are the simulated temperature distributions in the shield and the coils, respectively.

It can be seen that the temperature distribution in the shield is inhomogeneous and the temperature difference is 2.5 K. Fig. 5 shows that the temperature difference in the superconducting coils is less than 0.1 K, and the temperature of the inner coil is slightly higher than that of the outer coil, which is due to the fiberglass layers between the two coils.

The temperature difference between the second stage and the top end plate of the magnet is simulated as 0.2 K, resulting from the thermal resistance of the copper braid as well as the thermal contact resistance in the interfaces.

4. AC losses during charging

It is complex to accurately calculate AC losses in real situations. In this paper, we make a ballpark estimate based on some widely-accepted empirical formulas in [15], [16]. Because of the tiny slot in the brass former, the eddy current loss is very small and is ignored during charging [17]. The AC losses considered here include hysteresis loss and coupling loss. Each loss contribution is calculated separately, and the total AC losses are treated as the sum of these contributions.

The hysteresis loss P_{hy} (W/m^3) is estimated by:

$$P_{hy} = \frac{4}{3\pi} J_c r_f \left(\frac{dB}{dt}\right)\left(1+\left(\frac{J_{op}}{J_c}\right)^2\right) \qquad (5)$$

where r_f is the filament radius of the superconducting wires; dB/dt is the changing rate of flux density; J_{op} and J_c are the operating and critical current densities, respectively. J_c is a function of temperature and flux density, which is described in Fig. 6.

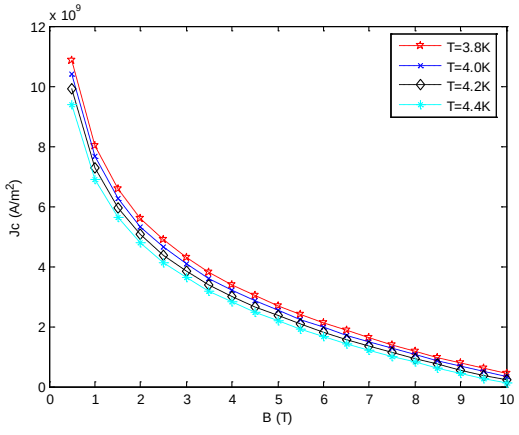

Fig. 6 – Critical current density of NbTi superconductor with respect to the flux density under different temperatures

The coupling loss P_{cp} (W/m^3) is calculated based on:

$$P_{cp} = \frac{2\tau}{\mu_0}\left(\frac{dB}{dt}\right)^2 \qquad (6)$$

where μ_0 is the air permeability and τ is the time

constant which is defined by:

$$\tau = \frac{\mu_0 l_p^2}{8\pi^2 \rho_e} \quad (7)$$

where l_p is the twist pitch and ρ_e is the effective resistivity of superconducting wires.

The calculated AC losses with respect to elapsed time during charging are plotted in Fig. 7. Two different current ramping rates are investigated here: 0.02 A/s and 0.015 A/s.

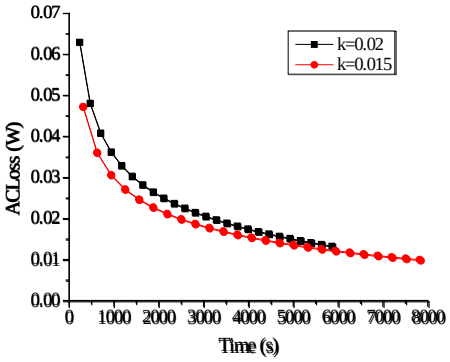

Fig. 7 – Calculated AC losses during charging

5. Thermal Tests

5.1. Cooling down

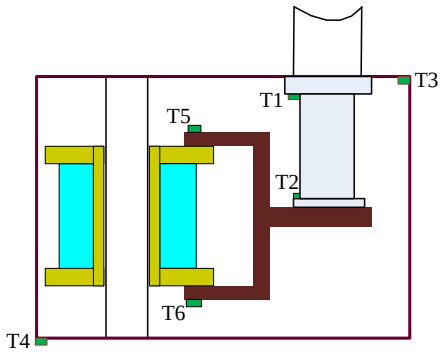

Fig. 8 – Locations of temperature sensors

The system is equipped with six temperature sensors. The locations of these sensors are indicated in Fig. 8. The cryocooler started working when the cryostat was pumped down to the range of 10^{-4} mbar. It took approximately 80 hours to cool the magnet from room temperature to the 4 K level.

Fig. 9 shows the cooling process of the system. After the system was stabilized, the temperatures T5 at the top end plate and T6 at bottom end plate reached 6.4 K and 4.8 K, respectively. The temperatures T1 in the first stage and T2 in the second stages were 52.1 K and 3.5 K, respectively. T5 was 1.8 K higher than T6, which was also observed in other repeated tests. It was speculated that the temperature sensor at the top end plate of the magnet was not installed or calibrated properly.

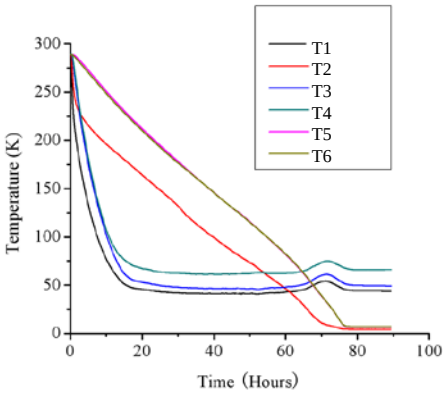

Fig. 9 – Cooling process of the system

5.2. Charging

The current was increased by 0.02 A/s up to 80 A, and then by 0.015 A/s to 105.5 A. The temperatures of the second stage and the magnet versus time during charging are shown in Fig. 10. It can be seen that the AC losses result in a temperature increase of 0.7 K in the magnet. The big difference between T5 and T6 could be due to improper installation or calibration of the temperature sensor.

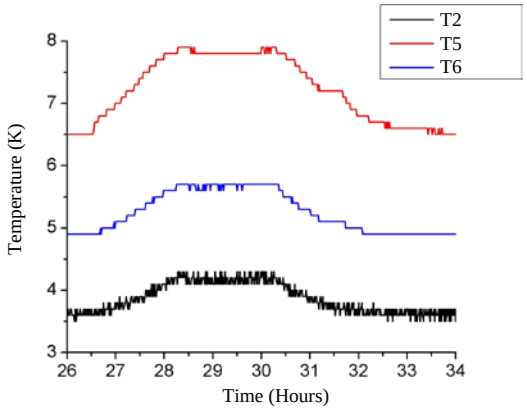

Fig. 10 – The temperature increase during charging. T2, T5, T6 are the temperatures in the second stage, top end plate and bottom end plate, respectively.

6. Conclusions

A conduction-cooled superconducting magnet system with a Ø 250 mm warm bore was successfully fabricated. The superconducting magnet could steadily transport a current of 105.5 A and generate a maximum central field of 4.5 T. The heat loads of the first and second stages were 15.2 W and 0.3 W, respectively. The AC losses during charging resulted in a temperature increase of 0.7 K in the magnet. The performance of the system was proved to be satisfying.

7. Acknowledgement

The authors express gratitude to the Division of Superconducting Magnet Science and Technology, IEE, CAS. They would also like to thank Matthew Lee Henriksen and Zhaoxi Liu in the Center for Electric Power and Energy (CEE), DTU, for their technical discussion and proofreading.

8. References

[1] Q. Wang, L. Yan, and B. Zhao, "Development of wide-bore conduction-cooled superconducting magnet system for material processing applications," *IEEE Trans. Appiled Supercond.*, vol. 14, no. 2, pp. 372–375, 2004.

[2] Q. Wang, Y. Dai, B. Zhao, and X. Hu, "Design and test of conduction-cooled high homogenous magnetic field superconducting magnet for gyrotron," *IEEE Trans. Appiled Supercond.*, vol. 17, no. 2, pp. 2319–2322, Jun. 2007.

[3] S. Chen, Y. Dai, B. Zhao, and Y. Li, "Development of an 8-T Conduction-Cooled Superconducting Magnet With 300-mm Warm Bore for Material Processing Application," *IEEE Trans. Appiled Supercond.*, vol. 24, no. 2, pp. 72–76, Apr. 2014.

[4] Y. Dai, L. Yan, B. Zhao, and S. Song, "Tests on a 6 T conduction-cooled superconducting magnet," *IEEE Trans. Appiled Supercond.*, vol. 16, no. 2, pp. 961–964, Jun. 2006.

[5] Y. Choi, D. Kim, and B. Lee, "Conduction-cooled superconducting magnet for material control application," *IEEE Trans. Appiled Supercond.*, vol. 19, no. 3, pp. 2190–2193, Jun. 2009.

[6] M. Hoenig, "Design concepts for a mechanically refrigerated 13 K superconducting magnet system," *IEEE Trans. Magn.*, vol. MAG-19, no. 3, pp. 880–883, 1983.

[7] Q. Wang, Y. Dai, and H. Huang, "Development of conduction-cooled high temperature superconducting magnet," *IEEE Trans. Appiled Supercond.*, vol. 15, no. 2, pp. 2332–2335, Jun. 2005.

[8] Y. Zhou, H. Wang, and Y. Dai, "Conduction-cooled superconducting magnet with 250 mm bore size," *IEEE Trans. Appiled Supercond.*, vol. 21, no. 3, pp. 2287–2290, 2011.

[9] Q. Wang, Y. Dai, B. Zhao, S. Song, S. Chen, L. Yan, Y. Bai, and K. Kim, "Design of superconducting magnet for background magnetic field," *IEEE Trans. Appl. Supercond.*, vol. 18, no. 2, pp. 548–551, 2008.

[10] Y. Choi, D. Kim, H. Yang, B. Lee, and W. Jung, "Cryocooled cooling system for superconducting magnet," *Proc. 15th Int. Cryocooler Conf.*, pp. 665–670, 2009.

[11] http://www.cryogenics.nist.gov/

[12] J. He, Y. Tang, J. Li, L. Ren, J. Shi, J. Wang, R. Qu, L. Su, X. Li, Y. Xu, and Z. Zhu, "Conceptual Design of the Cryogenic System for a 12 MW Superconducting Wind Turbine Generator," *IEEE Trans. Appl. Supercond.*, vol. 24, no. 3, pp. 1–5, Jun. 2014.

[13] G. White, *Experimental Techniques in Low-Temperature Physics*. 1979.

[14] ANSYS Manuals.

[15] Martin N. Wilson, *Superconducting Magnets* .

[16] Y. Iwasa, *Case Studies in Superconducting Magnets* .

[17] H. Y. M. Morita, "Stability analysis in cryogen-free superconducting magnets during current excitation," *Proc. 15th Int. Conf. Magn. Technol.*, pp. 1410–1413, 1997.